



RADIOCARBON DATING OF ORGANIC-RICH DEPOSITS: DIFFICULTIES OF PALEOGEOGRAPHICAL INTERPRETATIONS IN HIGHLANDS OF RUSSIAN ALTAI

R.K. NEPOP^{1,2}, A.R. AGATOVA^{1,2}, M.A. BRONNIKOVA³, E.P. ZAZOVSKAYA³,
I.YU. OVCHINNIKOV¹, P. MOSKA⁴

¹*Institute of Geology and Mineralogy SB RAS, Koptyuga av., 3, 630090 Novosibirsk, Russia*

²*Ural Federal University, Mira str., 19, 620002 Yekaterinburg, Russia*

³*Institute of Geography RAS, Staromonetny str., 29, 119017 Moscow, Russia*

⁴*Institute of Physics, Silesian University of Technology, Gliwice, Poland*

Received 10 November 2019

Accepted 28 August 2020

Abstract

The high mountainous southeastern part of Russian Altai is characterized by complicated sedimentation history. As a result of tectonic movements, Paleogene, Neogene, and even more old Carboniferous and Jurassic organic-rich deposits had been partly uplifted and exhumed on the ridge's slopes, where during the Pleistocene, they were affected by various exogenous processes including glaciation, glacio-fluvial erosion, winnowing activity of ice-dammed lakes, sliding during lake-draining events, followed by further intensive Holocene erosion, pedogenesis, and permafrost formation/degradation.

Remobilized ancient organic matter had been involved into geomorphic and pedogenesis processes and affected the results of radiocarbon dating. Numerous radiocarbon ages obtained revealed several typical problems in interpretation of dating results, which was confirmed by multidisciplinary investigations of associated sediments in a wider regional context.

This article presents a discussion on obtained apparent radiocarbon dates of organic material from ten sections of the SE Altai. In addition to radiocarbon analysis, in each case multidisciplinary study was carried out in order to properly interpret obtained dates, as well as to explain the inability of directly using apparent ¹⁴C ages as a geochronological basis for paleogeographical reconstruction. The analysis presented is of vital importance for establishing the chronology of formation of large ice-dammed lakes and their cataclysmic draining; revealing chronology and paleoenvironmental conditions of pedogenesis in the highlands of the SE Altai; and estimating the range and magnitude of the tectonically driven topography rebuilding in the post-Neogene time.

Keywords

radiocarbon dating, pedogenesis, ice-dammed lakes, outburst floods, paleogeographical reconstructions, Russian Altai.

1. Introduction and setting a problem

The Altai Mountains are the northern segment of the Central Asian collision belt (Fig. 1). They stretch northwest for more than 1500 km across the borders of Mongolia, China, Kazakhstan, and Russia and form a wedge shape narrowest in the southeast (about 50 km) and widest in the northwest (up to 500 km). The elevation increases southwest from 400 to 4000 m a.s.l. The mountain system has a Cenozoic age, but

to a large extent inherits the position of mountain structures that existed here in Permian and Jurassic times (Dobretsov *et al.*, 1996; Novikov, 2004; Glorie *et al.*, 2011, 2012).

Southeastern part of the Russian Altai (SE Altai) presented in this study is the highest and most seismically active part of the Russian Altai. It includes the Chuya and Kurai intermountain depressions, located at about 1750–2100 and 1470–1650 m a.s.l. correspondingly, and framing ridges with the altitudes in the range of 2900–4200 m a.s.l.

Corresponding author: Anna Agatova
e-mail: agatr@mail.ru

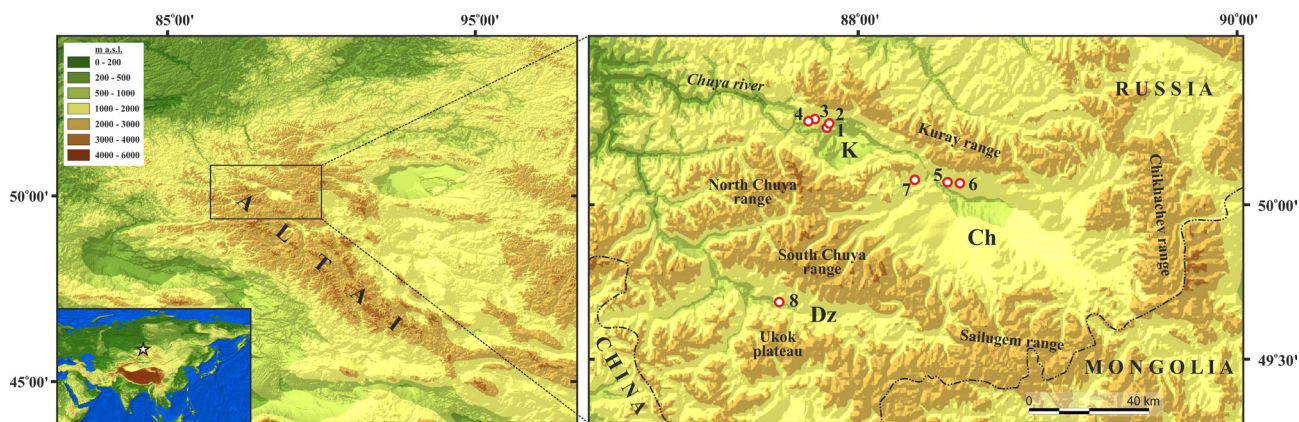


Fig 1. Location of the SE Altai within the Altai Mountains. The acronyms indicate the names of the largest intermountain depressions: Ch – Chuya, K – Kurai; Dz – Dzhazator valley. Red circles show the location of studied sections.

The area is characterized by strongly dissected topography – the result of Cenozoic orogenesis (Devyatkin, 1965; Novikov, 2004). Summits rise above the floors of intermountain depressions and major valleys up to 2600–3000 m, which is one of the largest values for the whole Altai Mountains (Agatova and Nepop, 2017).

The SE Altai is characterized by arid climate. The mean annual precipitation is less than 200 mm within the floor of the basins (Narozhny and Osipov, 1999). Nevertheless, due to the high altitudes of the ridges, the SE Altai is the center of the modern glaciation. Permafrost within the Chuya and Kurai intermountain depressions has a patchy distribution with the general thickness of 6–90 m and active layer of 3–7 m depth (Permafrost–hydrogeological map, 1977). Within the mountain ranges, unconsolidated sediments are frozen from a depth of about 0.8–1.5 m (Ostanin, 2007).

The Kurai–Chuya system of intermountain depressions of the SE Altai is the largest and oldest within the whole Altai Mountains. They are filled with redeposited products of Upper Cretaceous–Low Paleogene weathering crust, Paleogene–Neogene lacustrine and peat/brown coal boggy sediments, Pleistocene sediments (mainly alluvial, glacial, glacio-fluvial, glacio-lacustrine, and deposits associated with cataclysmic outburst floods from ice-dammed lakes), as well as with the Holocene deposits of various genesis.

Despite over 150 years of regional research history, the Quaternary paleogeography of the SE Altai is still debatable. Main concepts of the Pleistocene Altai glaciations vary from: *i*) the last glaciation (Sartan according to Western Siberian glaciation scheme or MIS-2) to be the largest among all Pleistocene glaciations and left the most prominent imprints in topography and sediments (Butvilovsky, 1993; Rudoy, 2005) to *ii*) the most extensive Middle Pleistocene glaciation followed by two Late Pleistocene glaciations with the most recent being the smallest one (Devyatkin, 1965). Differences in perceptions of the

number, chronology, and maximal extension of the Pleistocene Altai glaciations are closely related with the problems of the chronology and drainage mechanisms of extensive ice-dammed lakes in intermountain depressions, as well as with the issues of sedimentation patterns downstream along the Chuya and Katun river valleys.

In this context, numerical dating of various deposits and landforms is a key paleogeographical problem in the region. Today, the radiocarbon method is one of the most exploitable and widely applicable dating techniques. It allows determining the age of organic matter preserved/accumulated in deposits and is limited by ~50 ka. At the same time, a complicated tectonic and sedimentary regional history (which is generally typical for tectonically active mountain terrains) gives rise to the problem of interpretation of dating results. Tectonic movements cause exhumation of ancient (Carboniferous, Jurassic, Paleogene, and Neogene) organic-rich deposits on the ridge's slopes, where they are affected by various Pleistocene and Holocene exogenous processes. This is the reason for admixture of the “young” carbon into ancient organic material (with the own age beyond the limits of the radiocarbon method) and *vice versa*. As a result, applying radiocarbon dating technique in the SE Altai encountered the problem of obtaining apparent ^{14}C dates that reflect neither the age of the sediments nor the time of geomorphic processes that caused their redeposition. These apparent dates cannot be used as geochronological markers in paleogeographical reconstructions.

This article presents the examples of such apparent radiocarbon dates for the SE Altai. Their correct interpretation is critical to understand the Late Pleistocene landscape evolution and climate changes in the region including the following:

- i*) chronological reconstructions of Altai glaciations, associated ice-dammed lakes formation, and their cataclysmic draining;

- ii) establishing the chronology and paleoenvironmental conditions of soil formation in the highlands of the SE Altai;
- iii) estimating the range and magnitude of the tectonically driven topography rebuilding in the post-Neogene time.

In this context, we summarize the results of our previous investigations in the Kurai basin and Dzhazator valley, as well as analyze new data on deposits and pedogenesis in the Chuya basin. Together with the results of radiocarbon dating applying both accelerated mass spectrometry (AMS) and liquid scintillation counting (LSC) techniques, we present the results of multidisciplinary investigations of dating material. To provide independent age control, optically stimulated luminescence (OSL) technique was applied. Discussed problems in obtaining apparent ^{14}C dates have not been previously taken into consideration in regional investigations, but they are of vital importance to understand the Late Pleistocene paleogeography of the SE Altai.

2. Methods

Multidisciplinary investigations with the main focus on the Late Pleistocene chronological reconstructions and assessing the validity of the obtained radiocarbon dates were based on several methods. Geomorphological investigations and process analyses included the interpretations of space images, topographic maps, and field studies with mapping of landforms and deposits of different origin. Lithofacies analysis of studied sections was applied to understand the sedimentary environments and the origin of the exposed deposits.

The radiocarbon dates were obtained by the LSC method at the Institute of Geology and Mineralogy SB RAS, Novosibirsk (SOAN), and at the Laboratory of Radiocarbon Dating and Electronic Microscopy of the Institute of Geography RAS, Moscow (IGAN). The production of lithium carbide and benzene synthesis was completed using the standard technique (Arslanov, 1987; Skripkin and Kovalyukh, 1997). The activity of ^{14}C was determined using the Quantulus-1220 liquid scintillation counters. Single date applying AMS technique was obtained at the University of Arizona, USA, with the sample preparation at the Laboratory of Radiocarbon Dating and Electronic Microscopy of the Institute of Geography RAS, Moscow (IGAN_{AMS}). All ^{14}C ages were normalized to $\delta^{13}\text{C}$ value of -25‰ . The conventional radiocarbon ages were calibrated (2σ standard deviation) by applying the OxCal v4.3.2 program (Bronk Ramsey, 2017), with the IntCal13 calibration data set (Reimer *et al.*, 2013). The article presents both the conventional (years BP) and the calibrated (cal BP) ^{14}C ages.

Samples for OSL dating were collected by driving steel tube into the sandy sediment. Further sample preparation

and measurements were carried out at the Luminescence Dating Laboratory, Silesian University of Technology, Gliwice, Poland (GdTL). High-resolution gamma spectrometry using a HPGe detector was used to determine the content of U, Th, and K in the sample. The activities of the isotopes present in the sediment were determined using IAEA standards RGU, RGTh, and RGK after subtracting background values from the detector. Dose rates were calculated using the conversion factors of Guerin *et al.* (2011). The method of Prescott and Stephan (1982) was used for the cosmic ray beta dose rate calculation. An automated Risø TL/OSL DA-20 reader was used for the OSL measurements of multigrain aliquots, each weighing ~ 1 mg. Equivalent doses were determined using the single-aliquot regenerative-dose protocol (Murray and Wintle, 2000). To calculate the luminescence ages, the central age model (CAM) of Galbraith *et al.* (1999) was applied.

In addition to ^{14}C and OSL dating, a set of techniques were applied to study dating sediments in order to understand specific climatic and paleoenvironmental features that indicate the time of their accumulation/redeposition. The mineral composition of substrate was studied by X-ray diffraction (XRD) and infrared (IR) spectroscopy settings (Fagel *et al.*, 2007; Solotchina *et al.*, 2009). Analysis of the biological composition of the sediments, with the main focus on micropaleontological analysis, was used for reconstructing the paleoecology of the lakes and characterizing the paleoenvironmental conditions of the sedimentation (Uspenskaya, 1986; Skrypnikova *et al.*, 2011). Additionally, fossil ostracods were analyzed to estimate the age of the sediments, which serve as a parent substrate for pedogenesis or were affected by redeposition. Pollen and spore assemblages, as well as nonpollen palynomorphs, were analyzed for discovering clear indicators of ancient (Pre-Quaternary) age of inclosing deposits. Reference pollen collection and pollen atlases (Kuprianova and Alyoshina, 1972; Beug, 2004) were used to identify pollen grains and spores, as well as special descriptions, pictures, and photographs (Shumilovskikh *et al.*, 2015; Jankovska and Komarek, 2000) to establish nonpollen palynomorphs.

3. Results

Generally, ten sections in eight locations were studied within the SE Altai in the Kurai (sections 1-4) and Chuya (sections 5-7) intermountain depressions and in the Dzhazator valley (sections 8a-8c) (Fig. 1). Available radiocarbon and OSL dates are presented in Tables 1 and 2 and Fig. 2.

3.1 Section 1 N50°09'10", E87°58'50", 1570 m a.s.l.

Section of lacustrine and underlying gravel deposits, associated with the outburst floods from ice-dammed lakes, of about 200 m long and up to 4 m high, is exposed along

Table 1. Radiocarbon dating results. Dating material is marked as *co* – coal; *ha* – humic acids; *pp* – paleopeat; *toc* – total organic carbon. Dates marked with asterisk are results of dating of humic acids obtained from one sample.

Laboratory code	Studied sections (fig. 1)	Applied technique	Dating material	¹⁴ C yr BP	Cal BP (2σ)	Confidence intervals %	Description
SOAN 9496	1	LSC	ha	3380±115	3920-3370	95.4	Fossil soil in subaerial pack above lacustrine deposits
SOAN 9502	1	LSC	pp	22070±450	27350-25600	95.4	Inclusions of peat in the upper diluvial pack
SOAN 7802	1	LSC	ha	34750±480	40430-38370	95.4	Inclusions of organic matter in the middle part of upper diluvial pack
SOAN 4971	1	LSC	ha	20750±220	25560-24410	95.4	Fragment of charcoal in the middle part of upper diluvial pack (Vysotsky 2009)
SOAN 9503	1	LSC	pp	26715±700	32500-29360	95.4	Inclusions of peat at the bottom of the upper diluvial pack
SOAN 9306	1	LSC	ha	12400±195	15220-13920 13890-13860	94.8 0.6	Organic fragments in the lower diluvial pack (after Vysotsky in Agatova <i>et al.</i> , 2020)
SOAN 9305	1	LSC	ha	7320±110	8370-7950	95.4	Organic fragments in the lower diluvial pack (after Vysotsky in Agatova <i>et al.</i> , 2020)
IGAN 4811	2	LSC	pp	35090±950	41830-37700	95.4	Upper Oligocene–Low Miocene peat of Koshagach Formation
SOAN 9505	3	LSC	ha	33790±1095	40930-35820	95.4	Thin peat layer in sediments of the Early Holocene flowing paleolake
IGAN 3204	4	LSC	ha	18800±270	23420-22110	95.4	Upper peat layer (after Rogozhin <i>et al.</i> 2008)
SOAN 9575	4	LSC	ha	29375±285	34070-32910	95.4	Middle peat layer
SOAN 9576	4	LSC	ha	27970±320	32760-31200	95.4	Lower peat layer
SOAN 9689	5	LSC	ha	-	-	-	Silt loams at the same location as Beta 159972 sample (not enough material – 0.4g of ha from a 3-kg sample)
IGAN _{AMS} 7821	5	AMS	toc	21410±60	25900-25580	95.4	Silt loams at the same location as Beta 159972 sample
Beta 159972	5	AMS	ha	35870±490	41540-39470	95.4	Layer of organic sediment, probably part of paleosol profile (Herget, 2005)
IGAN 6249	6	LSC	ha	13990±270	17710-16210	95.4	Horizon [B] of fossil soil at the bottom of proluvial–coluvial pack
IGAN 6008	6	LSC	co	9830±230	12100-10580	95.4	Lens of charcoals under fossil soil
SOAN 9573-1	6	LSC	co	8635±150	10180-9400 9350-9330	95.1 0.3	Lens of charcoals under fossil soil
SOAN 9573-2	6	LSC	ha	9220±95	10660-10620 10610-10220	1.9 93.5	Matrix in lens of charcoals under fossil soil
IGAN 5011	7	LSC	co	50120±2300	-	-	Upper Oligocene–Low Miocene brown coal of Koshagach Formation from Taldy–Dyurgun deposit
IGAN 4880	8a	LSC	pp	44790±1400	-	-	Upper layer of brown coal
IGAN 4881	8a	LSC	co	37570±1100	44000-40060	95.4	Lower layer of brown coal
SOAN 9495	8b	LSC	pp	14085±400	18140-16020	95.4	Upper (among three) interlayers within the peat horizon
IGAN 4908	8b	LSC	pp	36680±910	42730-39550	95.4	Lower (among three) interlayers within the peat horizon
SOAN 8709	8c	LSC	ha	2760±80	3070-2740	95.4	Upper partly exhumed at the surface organic mineral layer
SOAN 8420	8c	LSC	ha	23100±415	28080-26440	95.4	
SOAN 8421	8c	LSC	ha	25530±355	30620-28880	95.4	
SOAN 8422	8c	LSC	ha	16600±140	20410-19640	95.4	
SOAN 8710	8c	LSC	ha	15330±110	18820-18340	95.4	
SOAN 8711*	8c	LSC	ha	17940±120	22090-21370	95.4	
SOAN 9464*	8c	LSC	ha	22475±450	27570-25940	95.4	Layers of organic mineral matter with inclusions of organic material (mainly fragments of peat and sometimes lignitized wood) affected by solifluction
SOAN 9627*	8c	LSC	ha	22880±280	27670-26540	95.4	
SOAN 8712**	8c	LSC	ha	15600±100	19080-18630	95.4	
SOAN 9467**	8c	LSC	ha	26400±500	31300-29500	95.4	
SOAN 9629**	8c	LSC	ha	19480±360	24310-22600	95.4	

Table 2. OSL dating results. The dose rate was determined based on the radioisotope content measurements. The equivalent doses were calculated using central age model (Galbraith et al., 1999). OSL age is given with 1σ standard deviation except samples GdTL 3125 and GdTL 3126 (2σ).

Laboratory code	Sample location (fig. 1)	U (Bq/kg)	Th (Bq/kg)	K (Bq/kg)	Dose rate (Gy/ka)	Equivalent dose (Gy)	OSL Age (ka)	Number of aliquots	Water content	Sample description
GdTL 2590	1	29.1±0.8	22.4±0.5	434±14	2.21±0.08	42.0±1.8	19.0±1.1	13	18±5%	Sandy layer at the top of cross-bedded diluvial pack (Fig. 3)
GdTL 2591	1	25.3±0.6	20.0±0.4	485±15	2.23±0.08	35.9±3.5	16.0±1.7	20	18±5%	Sandy layer between horizons of loams (Fig. 3)
GdTL 3125	3	16.6±0.4	21.4±0.6	480±23	2.06±0.09	19.6±1.5	9.41±1.68	12	18±5%	Lacustrine sands below the peaty layer (Fig. 5)
GdTL 3126	3	17.3±0.4	21.9±0.7	486±26	2.11±0.09	23.6±1.5	11.12±1.74	14	18±5%	Lacustrine sands above the peaty layer (Fig. 5)
GdTL 3424	5	17.2±0.8	24.0±1.2	501±42	2.20±0.18	81.2±2.7	37.0±3.1	27	15±5%	Sandy layer at the bottom of sliding proluvium (Fig. 7)

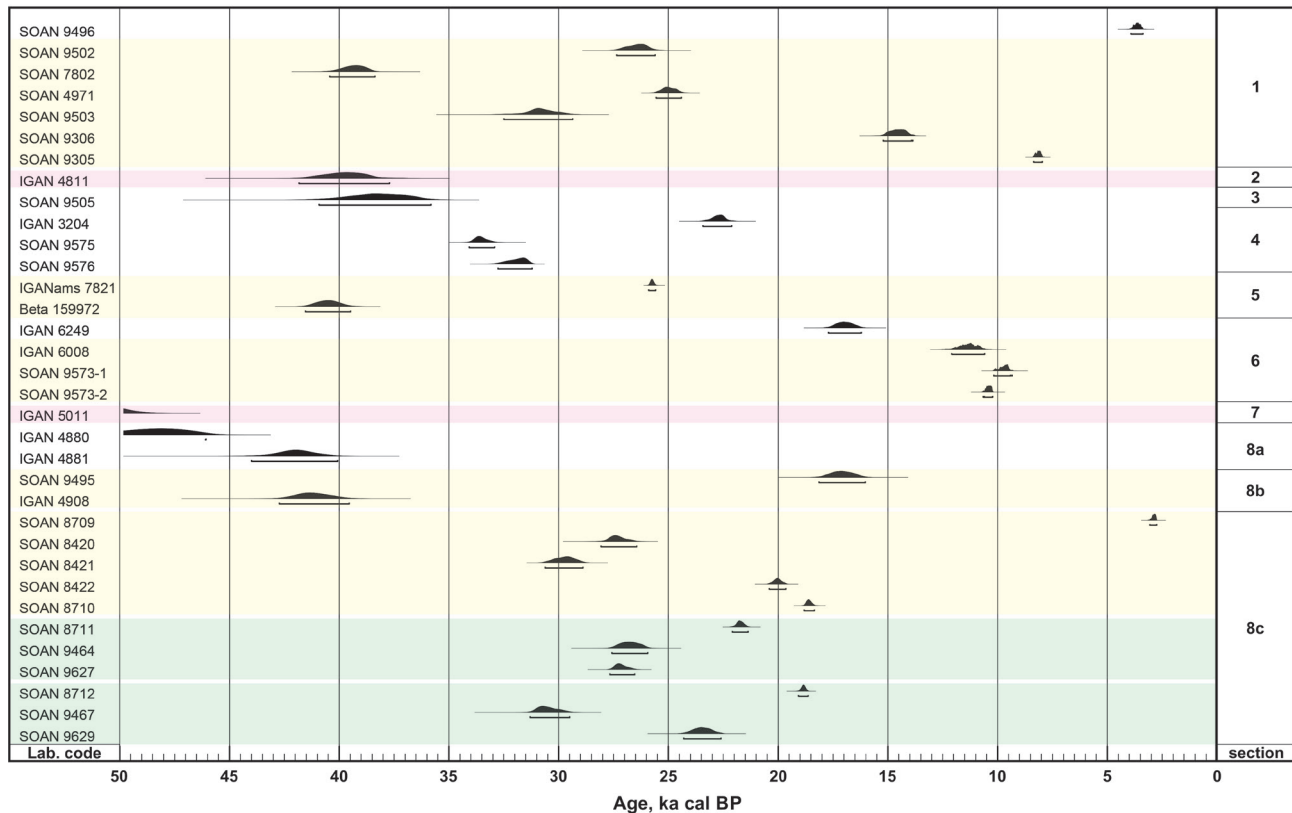


Fig 2. Multiplot view of analyzed radiocarbon ages. Dating results are marked as follows: red – for the samples collected in ancient (Upper Oligocene–Low Miocene peat and brown coal-bearing) deposits; yellow – for the samples collected from the single pack of sediments; and green – for dating results of humic acids obtained from one sample.

“the Chuya-highway” on the slope of the small neotectonic protrusion (foreberg) at the foot of the Kurai range in the northwestern part of the Kurai intermountain depression (Fig. 3a). The artificial outcrop reveals the detailed stratigraphy of the 1570-m a.s.l. strandline of about 100 m width, which is one of the lowest preserved strandlines within the Kurai basin (Fig. 3b). The diluvial (e.g., cataclysmic flood)

deposits are represented by two sequences of pebbles, granules, gruss, and coarse and medium-grained sands: the lower one is with horizontal bedding; the upper one, obliquely bedding with boulder lenses at the base. The presence of a large amount of carbonized organic inclusions is typical for both diluvial sequences (Fig. 3c). Lacustrine deposits in Section 1 are represented by two overlying horizons of

sandy loam (with a total thickness of 50–80 cm), where fragments of fish scales and a large number of freshwater ostracods were detected (Agatova *et al.*, 2020). The sub-aerial pack above the lacustrine pack includes buried soil horizon.

The OSL ages of 19.0 ± 1.1 ka (GdTL 2590) and 16.0 ± 1.7 ka (GdTL 2591) for sandy layers below and between the horizons of loams, together with the radiocarbon age of 3920–3370 cal BP (SOAN 9496) for buried soil above the lacustrine deposits indicate the formation of the last ice-dammed lake and rapid draining of the preceding lake in the Kurai basin during Sartan (MIS-2) time (Fig. 4). Four ^{14}C ages for the organic material from the upper diluvial sequence fall within a wide time interval of 24.4–40.4 ka cal BP. Additionally, radiocarbon dating from the lower

diluvial pack returned younger and stratigraphically inconsistent ages of about 14.5 and 8.2 ka cal BP.

3.2 Section 2 N50°15'32", E87°54'58", 1645 m a.s.l.

Section 2 is located within the same neotectonic protrusion and exhibits the Upper Oligocene–Low Miocene peat and brown coal-bearing deposits in natural outcrop of a dry gully about 1.5 km northwest of Section 1 (Fig. 5). These deposits were exhumed to the surface and were affected by winnowing activity of the Late Pleistocene ice-dammed lakes. This is one of the possible sources of ancient organic material. Apparent ^{14}C age of 41830–37700 cal BP (IGAN 4811) of brown coal-bearing Oligocene–Miocene deposits demonstrates the discrepancy between obtained radiocarbon date and paleontological and geochemical features of the studied sediments.

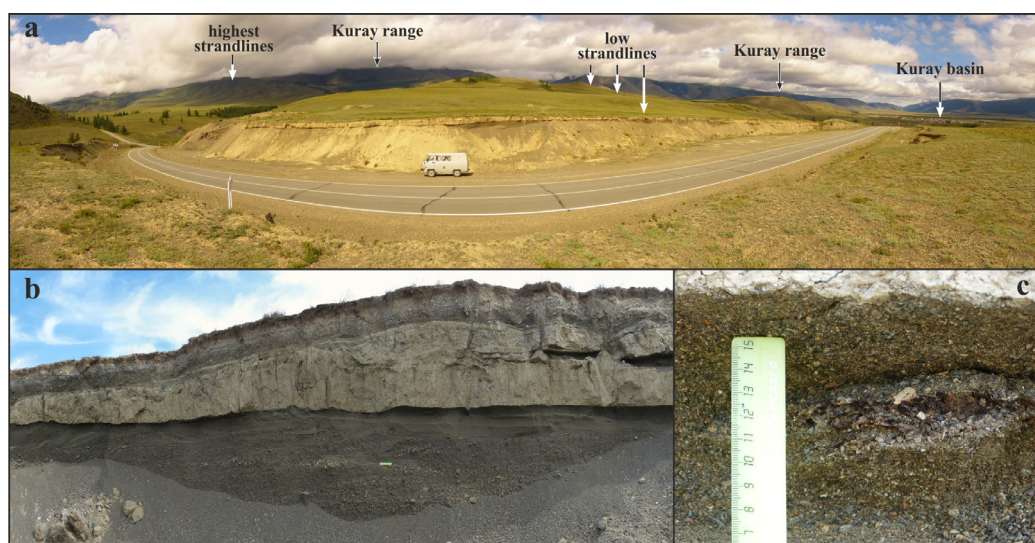


Fig 3. Geomorphological position of Section 1 (a), west–east stretch of sediments (b) along the roadcut in a strandline at altitude of ~ 1570 m a.s.l. and numerous fragments of organic matter (c) presented in diluvial deposits as inclusions. Field car is 2 m high and 4 m long.

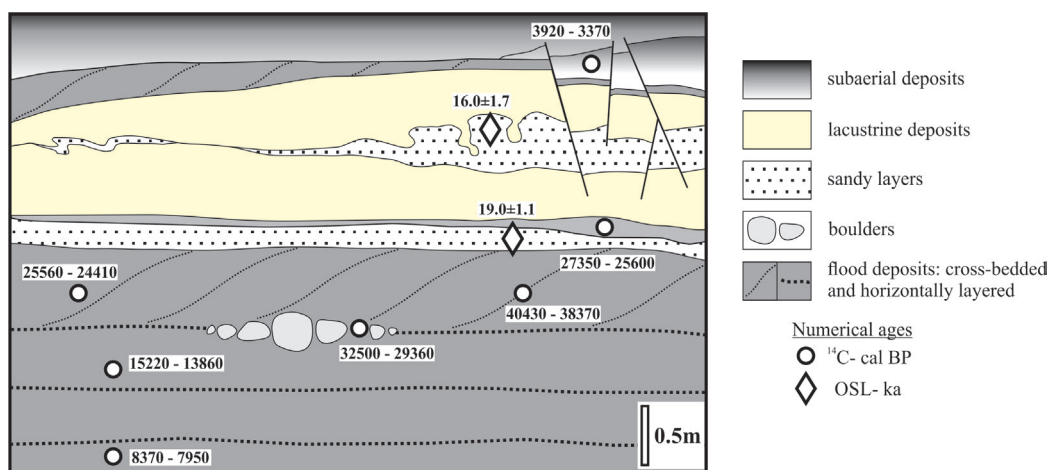


Fig 4. Generalized scheme of sedimentary records in Section 1 and available numerical ages.

3.3 Section 3 N50°14'00", E87°42'29", 1480 m a.s.l.

Artificial outcrop along a roadcut of the “Chuya-highway” (section 3, Fig. 6) was studied within the western periphery of the Kurai basin near its outlet. Section 3 reveals the structure of the erosion terrace cut in the lacustrine sediments. It represents horizontally bedded fine and medium sands, which were accumulated in a flowing lake. Sands include several clay layers with ostracod fauna and a single thin (less than 1 cm) layer of peaty material. Along the section, peaty layer breaks down into separate lenses and fragments. Peat was dated by applying radiocarbon method as 40930–35820 cal BP



Fig 5. The Upper Oligocene–Low Miocene peat and brown coal-bearing deposits exposed in Section 2. General view of the outcrop in a dry gully (a) and sample of ancient peats from the lower part of the section (b).

(SOAN 9505) (Agatova *et al.*, 2019). Two OSL dates were obtained for sands above and below it. Calculated with 2σ standard deviation, OSL ages are 9.41 ± 1.68 ka (GdTL 3125) and 11.12 ± 1.74 ka (GdTL 3126). It indicates the early Holocene time of lacustrine sedimentation, which is three–four times younger than the radiocarbon age of peat inclusions. Results of numerical dating argue for redeposition of ancient organic matter (whose age is most likely far beyond the limits of radiocarbon method) by recent geomorphic processes.

3.4 Section 4 N50°14'50", E87°50'20", 1580 m a.s.l.

The artificial outcrop is located on the left-bank terrace of a small stream (the right tributary of the Chuya River), which drains a narrow tectonic depression between the Kurai range and foreberg in the northwestern part of the Kurai basin (Fig. 7). Sedimentation record in this section reveals interbedding of alluvial and peat layers (up to 5–10 cm thick) and indicates periodical riverbed migration and accumulation of sediments with peat filling. Earlier, the upper among four organic-rich horizons was dated 23420–22110 cal BP (IGAN 3204) (Rogozhin *et al.*, 2008). The obtained radiocarbon ages for organic material from two underlying peat layers – 34070–32910 (SOAN 9575) and 32760–31200 (SOAN 9576) cal BP show inversion. As well as in the sections 1 and 3, washed out Paleogene–Neogene brown coal deposits most likely served as original source for peaty-rich horizons. Obtained ^{14}C ages fall within the pre-glacial and last glacial periods of the Pleistocene cold epoch and contradict to organic-rich sedimentation in the high mountainous environment. Apparent character of these radiocarbon ages is also confirmed by small thickness of alluvium, which assumes shorter (than ~ 10 ka) accumulation time for the upper alluvial layer. Additionally, in contrary to the obtained Pleistocene ages, sediments in Section 4 are not affected by winnowing activity of the last ice-dammed lakes.

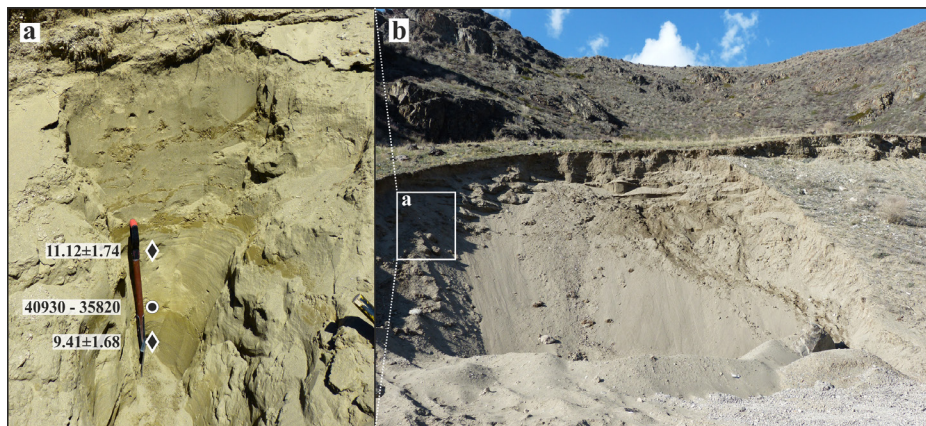


Fig 6. General view of the outcrop (b), exposed sediments, and obtained numerical ages (b) for Section 3. Sample location and calculated ages are indicated by rectangle for OSL (ka) and by circle for ^{14}C (cal BP) dates.



Fig 7. Geomorphological position of Section 4 (a). View to southwest along the “Chuya-highway”. North Chuya range in the background. Exposed sediments and available radiocarbon dates for peaty-rich layers (b).

Next two sections (5 and 6) are located in the north-western periphery of the Chuya intermountain depression, in the valleys of temporal creeks, which drain the southern slope of the Kurai range. In this part of the Chuya basin, Jurassic, Paleogene, and Neogene organic-rich lacustrine and boggy-lacustrine deposits, including interbeds of brown coals, are widely exposed at the surface, and, according to drilling and geophysical studies, are traced under Quaternary deposits (Devyatkin, 1965; Nekhoroshev, 1966; Luzgin and Rusanov, 1992; Buslov *et al.*, 1999; Shokalsky *et al.*, 1999; Selin and Goverdovsky, 2000; Nevedrova *et al.*, 2001; Deev *et al.*, 2012). Sliding and redeposition of Paleogene–Neogene deposits at the foot of the Kurai range in this part of the basin has an areal distribution. Location 7 (Fig. 1) also marks the Taldy–Dyurgun deposit of the Upper Oligocene–Low Miocene brown coals in the western periphery of the Chuya basin.

3.5 Section 5 N50°03'31", E88°26'34", 1783 m a.s.l.

Section 5 presents a natural outcrop on the left slope of a short gully, which cuts the left slope of the Kamsug valley (Fig. 8). The upper reaches of the Kamsug valley cut an extended area, where Paleogene and Neogene deposits are exposed along the Kurai fault zone at the foot of the Kurai range. Downslope the Kamsug valley cuts are gravel dunes associated with cataclysmic outburst floods from ice-dammed lake in the Chuya basin. In Section 5, deep-angled (18°) cross-bedded layers of gravels and pebbles (up to 2.3 m thickness) rest unconformably on the eroded surface of proluvial deposits.

The proluvial pack is represented by well-stratified loams and sandy loams opened to a depth of about 0.9 m. Inclination of the layers and irregular boundaries between them, turbations, involutions, presence of disoriented lenticular aggregates, etc., testify the later involvement of proluvium into a short-distant solifluctional transportation down the paleo-slope. Definite pedogenic features are evidence of soil formation on the paleosurface of proluvium. Among them are well-developed structures resulted from ice segregation processes, redoximorphic features, and

clay coatings. Studied paleosol profile lacks its topsoil and relates to [B] horizons of permafrost-affected soils with satisfactory water supply.

The [B] horizon of the buried soil contains insufficient amount of organic matter for applying LSC ^{14}C dating (after preparation, a 3-kg sample SOAN 9689 showed only 0.4 g of humic acids). Radiocarbon dating of total organic carbon from this location applying AMS technique returned the age 25900–25580 cal BP (IGAN_{AMS} 7821), which is significantly younger than previously published AMS ^{14}C date 41540–39470 cal BP (Beta 159972, Herget, 2005). Large scattering of radiocarbon ages is related to a mixture of heterogeneous and heterochronous organic matter pools in dating samples. The Paleogene–Neogene age of the redeposited parent substrate is confirmed by its mineralogical composition and by pollen spectra. Pre-Quaternary conifer pollen, including *Tsuga*, predominates in pollen spectra, which include also pollen grains of broadleaf trees. This vegetation had completely disappeared in the region by the beginning of the Pleistocene. OSL date 37.0 ± 3.1 ka (GdTL 3424) for the underlying sandy layer predates the Pleistocene pedogenesis in this location, as well as formation and cataclysmic draining of the last ice-dammed lake in the Chuya basin.

The influx of “young” carbon into organic sediments, which contain geological carbon, was demonstrated by obtaining the count of ^{14}C date 50120 ± 2300 years BP (IGAN 5011) for the Upper Oligocene–Low Miocene brown coal from the Taldy–Dyurgun deposit (location 7, N 50°05'13", E 88°20'14", 1807 m a.s.l., Fig. 9) in the Chuya basin. This is an obvious example of apparent ^{14}C age.

3.6 Section 6 N50°03'30", E88°31'27", 1890 m a.s.l.

Section 6 presents a natural outcrop on the left slope of a small erosion valley 5 km eastward from Section 5 (Fig. 10). This short valley (among other ones) cuts the Bigdon Hills, which are a tectonic protrusion at the foot of the Kurai ridge (Devyatkin, 1965; Novikov, 2004). The Bigdon Hills are dressed by Paleogene–Neogene

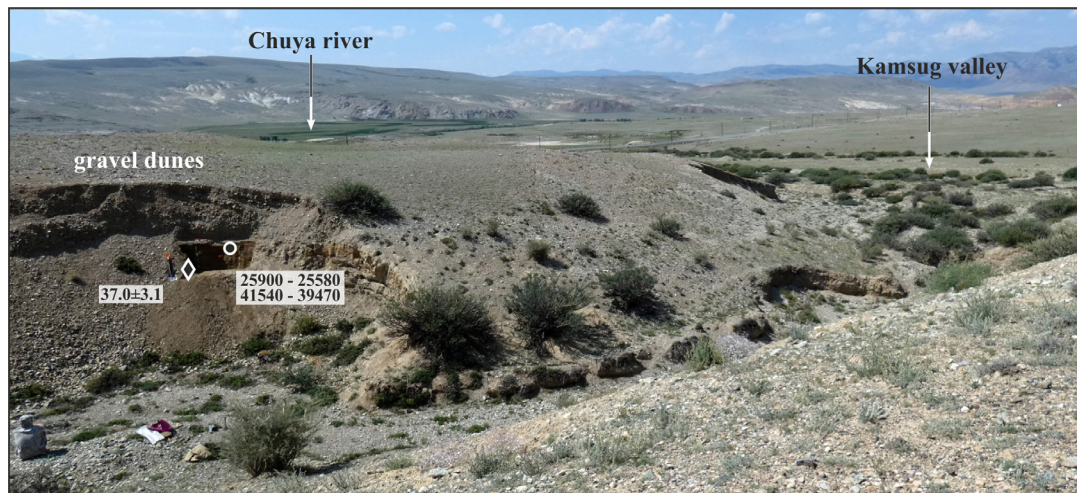


Fig 8. Geomorphological position of Section 5. Sample location and obtained numerical ages are indicated by rectangle for OSL (ka) and by circle for ¹⁴C (cal BP) dates.



Fig 9. Taldy-Dyurgun brown coal deposit.

lacustrine and boggy deposits (Nevedrova *et al.*, 2001; Deev *et al.*, 2012), characterized by the abundance of organic matter. The slopes of the Bigdon Hills are covered by the Pleistocene proluvial and lacustrine deposits and exhibit numerous strandlines associated with the Pleistocene ice-dammed lakes. Absence of lacustrine terraces on the bottom and lower parts of the slopes in these erosion valleys argues for their deepening already after drying of ice-dammed reservoirs. Erosion scarp 12 m long and 3 m deep displays two packs: alluvium (~1.5 m thickness) and covering proluvial-colluvial deposits. The upper pack includes sandy loams – eroded horizons [B] of buried soils and lenses of humus sand with a large amount of charcoals at the base of the pack. Thus, lenses with charcoals lie stratigraphically lower than buried soils in the same section.

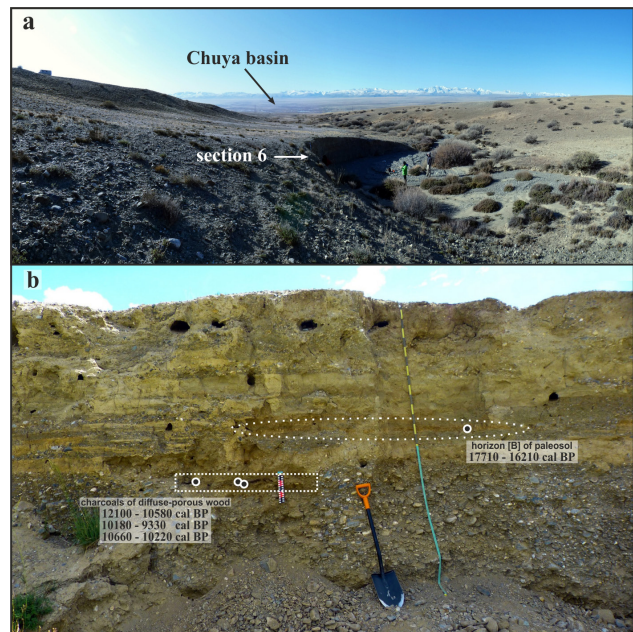


Fig 10. Geomorphological position (a), exposed sediments, and obtained radiocarbon ages (b) for Section 6.

Radiocarbon dating of the lowest [B] horizon of buried soil returned the age 17710–16210 cal BP (IGAN 6249). Charcoal is one of the best materials for applying radiocarbon technique, and ¹⁴C ages of charcoals from the underlying lens of humus sand show 10180–9330 cal BP (SOAN 9573-1) and 12100–10580 cal BP (IGAN 6008). Dating of enclosing material returned the age 10660–10220 cal BP (SOAN 9573-2). Thus, there is an inversion of obtained radiocarbon ages of buried soil and charcoals. Radiocarbon dating result for paleosol in Section 6 returns erratic (aged) date due to the influx of ancient organic matter. It is note-

worthy that the ^{14}C age of the charcoal-containing substrate also turned out to be older than the ^{14}C age of the charcoals. This suggests a single mechanism for the influx of ancient organic material during the accumulation of the upper proluvial–colluvial pack.

Three sections (8a, b, c) presented below, where apparent radiocarbon dates were earlier reported (Agatova *et al.*, 2019), are located in the Dzhazator valley at the foot of the south slope of the South Chuya range.

Section 8a N49°41'54", E87°32'18", 1765 m a.s.l.

Section 8b N49°41'42", E87°31'55", 1691 m a.s.l.

Section 8c N49°41'18", E87°31'58", 1611 m a.s.l.

In the Dzhazator valley (Fig. 11a), the Upper Oligocene–Low Miocene brown coal-bearing Koshagach Formation is confined to the southern foot of the highest (up to 3936 m a.s.l.) part of the South Chuya range. Pleistocene tectonic movements caused uplifting of deposits on the ridge's slope and their further areal sliding (Agatova *et al.*, 2017). Cold lacustrine and transitional waters, associated with the degradation of the Pleistocene glaciations, also controlled the downslope sliding of substrate. Three sections (8a, b, c, Figs. 11b and 12a, b) with different state of transformation of the organic material were studied in this location. Coal-bearing layers in the upper Section 8a are least changed and are horizontally bedded. In the middle Section 8b, these layers are creased into folds, but with preserved internal structure. Finally, in the lower Section 8c, ancient organic material is redeposited with a high content of mineral matter. Deposits from all these sections are characterized by the Oligocene–Miocene pollen spectra, where *Tsuga* are presented in significant quantity. Geochemical analysis indicates the accumulation of organic material under warm climate, which significantly differed from the Pleistocene conditions.

Fifteen radiocarbon dates of both redeposited organics and lithified peat–brown coal layers with unbroken structure, obtained in three different laboratories, fell within the interval 16.0–50 ka cal BP (Fig. 2, Table 1), that is, Late Pleistocene. The only one exception is the age 3070–2740 cal BP (SOAN 8709) of the upper partly exposed peaty layer in Section 8c. It demonstrates the predominance of “young” carbon in dated organic matter as a result of modern pedogenesis. There is a large scattering of radiocarbon dates in all studied sections: 40.1–50 ka cal BP, 16.0–42.7 ka cal BP, and 18.3–31.3 ka cal BP (for sections 8a, 8b, and 8c, respectively). In sections 8a and 8c (with the most preserved and redeposited material correspondingly), there is also an inversion of radiocarbon ages. Additionally, scattering of obtained ages is observed not only for a single pack of sediments (up to 26.7 ka and 13.0 ka in sections 8b and 8c), but even for a single sample (Fig. 2). Dating of humic acids extracted from two samples, each of which was divided into three parts, returns broad ranges of calculated radiocarbon ages 21.4–27.7 ka cal BP (SOAN 8711, 9464, 9627) and 18.6–31.3 ka cal BP (SOAN 8712, 9467, 9629). Thus, all reported in sections 8a, b, c radiocarbon dates are apparent ages that reflect neither the age of the sediments nor the time of their redeposition.

4. Discussion

It should be noted that complicated sedimentation history in the SE Altai is generally typical for the tectonically active mountain uplifts of Central Asia. Being involved into geomorphic and pedogenesis activity of ancient organic matter of millions and even ten million years old penetrates

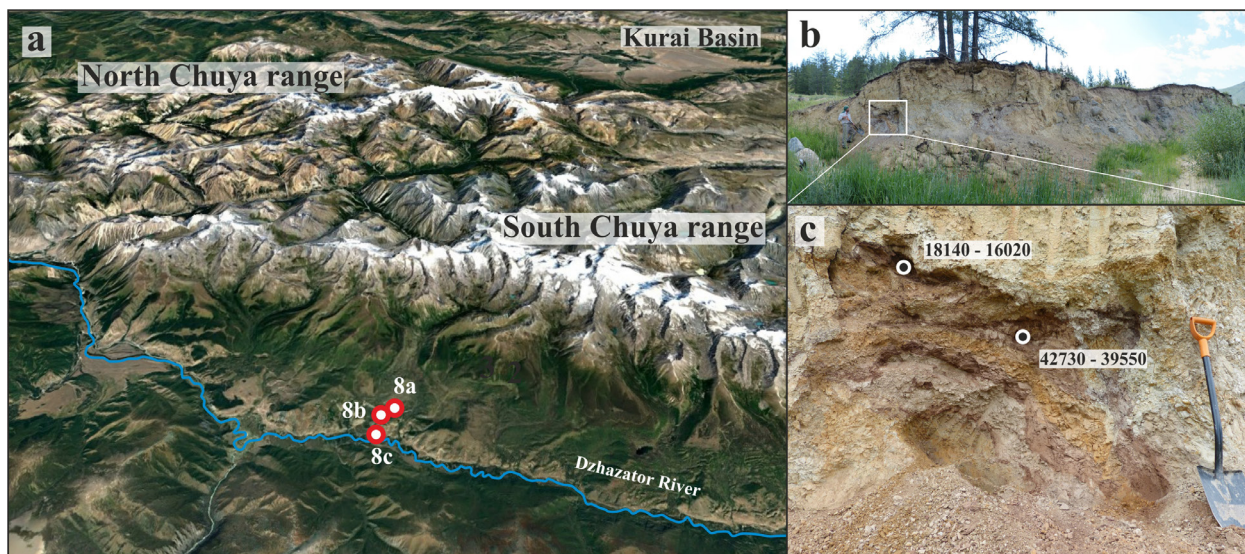


Fig 11. Google image of studied sites in the Dzhazator River valley (a); exposed sediments and obtained radiocarbon ages for Section 8b (b, c).

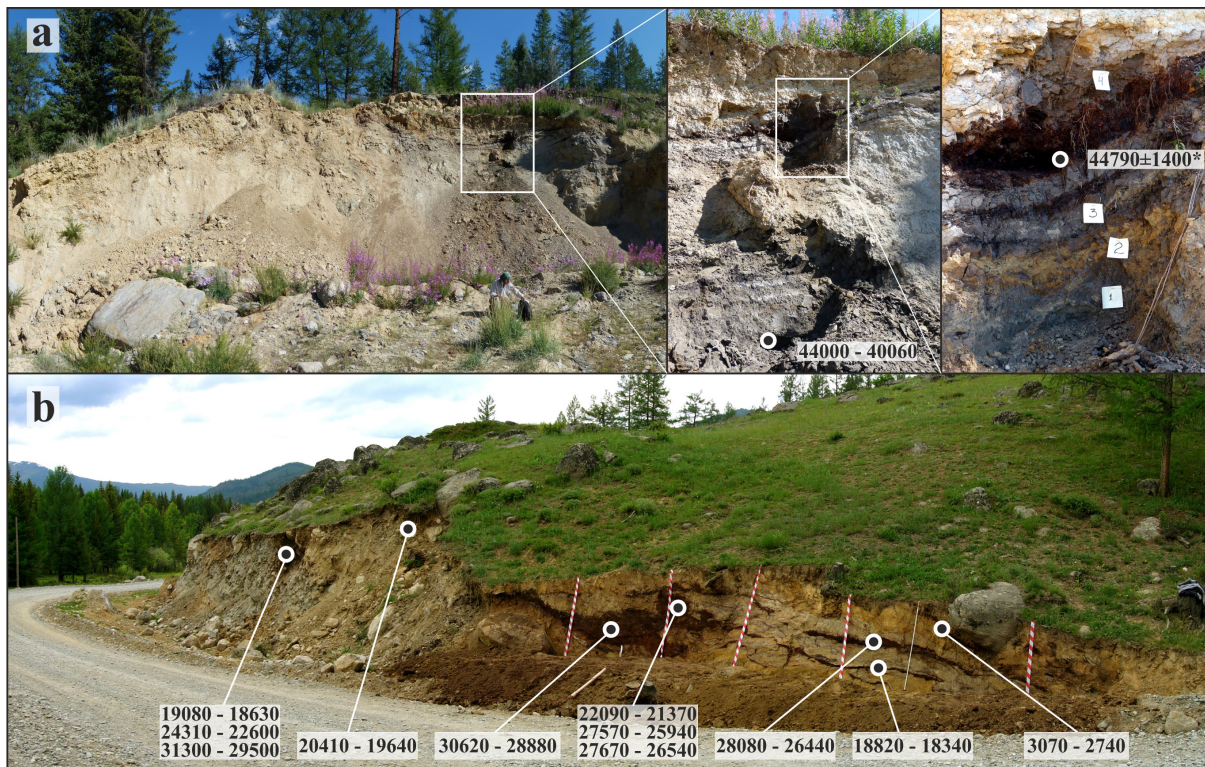


Fig 12. Exposed sediments and obtained radiocarbon ages for Section 8c (a); redeposited organic mineral material and obtained radiocarbon ages for Section 8a (b).

* indicates uncalibrated ^{14}C age for sample IGAN 4880 (see Table 1).

into young sediment or serves as a parent material for soil formation. Mixing of such originally different organic matter contributes to the final pool of organic carbon in dated samples and affects the results of radiocarbon dating. At the same time, apparent ^{14}C ages obtained often serve as chronological benchmarks in paleogeographical reconstructions without any discussion. Below, we discuss these dates in the context of specific highly debatable regional problems.

4.1 Chronological reconstructions of Altai glaciations, associated ice-dammed lake formation, and their cataclysmic draining.

As it was mentioned above, currently there are two major concepts of the Pleistocene Altai glaciations. The first one suggests the Last (MIS-2) Glaciation to be the largest among all Pleistocene glaciations which left the most prominent imprints in topography and sediments (Butvilovsky 1993; Rudoy, 2005). In contrast, Devyatkin (1965) supposed the most extensive Middle Pleistocene glaciation was followed by two Late Pleistocene glaciations, with the most recent being the smallest one. Following different concepts of Altai glaciations, there are also several chronological reconstructions of ice-dammed lakes in the Chuya–Kurai basins including the highly debatable issue of accumulation of the last reservoirs: *i*) In the upper reaches of the

Chuya River, the last shallow reservoirs existed as two separate lakes in the Kurai and Chuya basins at the end of MIS-2 (about 12–14 ka BP). Draining of these reservoirs is not believed to be associated with cataclysmic outburst floods (Okishev and Borodavko, 2001); *ii*) a single and the largest lake occupied the Chuya–Kurai basins during MIS-2 (Butvilovsky, 1993; Rudoy, 2002; Herget, 2005), and its cataclysmic draining occurred about 15–16 ka (Reuther *et al.*, 2006) (later ^{10}Be dates were recalculated to ca. 18 ka by Gribenski *et al.*, 2016); *iii*) alternatively, the Chuya and Kurai basins were dry since MIS-4, and there were no ice-dammed lakes, as well as cataclysmic outburst floods in the region in MIS-2 (Zolnikov and Mistrukov, 2008; Zolnikov *et al.*, 2016); *iv*) last ice-dammed lakes occupied the Kurai basin in MIS-2, but they were associated neither with the largest Pleistocene glaciations nor with the most powerful draining events. Outburst floods from these last (MIS-2) lakes were able to generate giant gravel dunes within the basin bottom (Agatova *et al.*, 2020).

Due to the lack of numerical age estimations for glacial and associated sediments, single ^{14}C dates (sometimes near or beyond the time limit of radiocarbon method) of organic inclusions in Pleistocene lacustrine and coarse deposits are used as geochronological markers (Svitoch *et al.*, 1978; Okishev and Borodavko, 2001; Zolnikov, 2011). Thus, the

conclusion about final drying of the Kurai basin before the Sartan (i.e., MIS-2) time (Zolnikov, 2011) was based on a single ^{14}C date 25560–24410 cal BP (SOAN 4971) originally reported by Vysotsky (2009) for organic inclusion collected from the cross-bedded layer in Section 1 (Fig. 4). At the same time, possible redeposition of ancient organic matter was not discussed, enclosing deposits were not dated, and the genesis of loams overlapping coarse-grained horizontal and cross-bedded sediments in this section was not studied.

The time of accumulation of the upper cross-bedded layer in this section is more confidently characterized by the OSL date 19.0 ± 1.1 ka (GdTL-2590) and is confirmed by the OSL age 16.0 ± 1.7 ka (GdTL-2591) of covering lacustrine deposits with fragments of fish scale and freshwater ostracod fauna (Agatova *et al.*, 2020). At the same time, four ^{14}C ages for the inclusions of organic material from the cross-bedded pack range between 24.4 and 40.4 ka cal BP. Radiocarbon dating of the lower horizontally bedded diluvial pack returned younger and stratigraphically inconsistent ages of about 14.5 and 8.2 ka cal BP. We argue that all discussed radiocarbon dates for organic inclusions in Section 1 are apparent ages. They evidence for mixing of “young” and “old” carbons in dated organic matter in a unique for each sample ratio. These dates do not reflect the true age of the organic matter, as well as the age of enclosing sediments. This example also demonstrates the importance of the detailed study of dated material as well as difficulties in interpretation of single dates.

Another example of a single radiocarbon date, which is of critical importance for regional paleogeography, is uncalibrated AMS ^{14}C age 35870 ± 490 BP (Beta 159972) reported by Herget (2005) in Section 5. This date was obtained for the top of the proluvial pack under cross-bedded diluvial sediment and predates the last ice-dammed lake in the Chuya basin and its cataclysmic draining. The silt layer nearby was dated applying OSL technique (~ 28 ka, BN 243) (Herget, 2005). Due to low optical quality and expressed low OSL sensitivity of quartz grains, dating was carried out with just a few aliquots, and, according to Wallinga (2002), could not be successful. So, radiocarbon date 35870 ± 490 BP (41540–39470 cal BP, Beta 159972) was used as a chronological benchmark for reconstructing the MIS-2 age of the maximal ice-dammed lake in the Chuya basin and its further cataclysmic draining (Herget, 2005; Herget *et al.*, 2020).

At the same time, its solitude and location of the studied section at the place of areal distribution of the Paleogene–Neogene deposits stipulated the importance of the multi-disciplinary study of dated organic matter. We argue for the Pleistocene time of the redeposition of Paleogene–Neogene substrate due to several reasons: *i*) The Paleogene–Neogene substrate exhibits traces of pedogenesis under cold

and humid conditions, which corresponds to Pleistocene climate; *ii*) pollen spectra contain a small percentage of pollen and nonpollen palynomorphs of Quaternary appearance; and *iii*) the redeposited Paleogene–Neogene substrate is covered by cataclysmic flood deposits associated with draining of the last Pleistocene ice-dammed lake. At the same time, the Paleogene–Neogene age of the parent substrate is confirmed by its mineralogical composition: Gypsum and goethite are clear characteristics of the Koshagach Formation (the Late Oligocene–Early Miocene), and dolomite is an exclusive feature of the Tueryk Formation (Middle Miocene–Middle Pliocene). Another strong evidence is pollen spectra that clearly indicate predominance of Pre-Quaternary pollen conifers, including *Tsuga* (23–24%), and presence of pollen grains of broadleaf trees that had completely disappeared in the region by the beginning of the Pleistocene.

New AMS ^{14}C date 25900–25580 cal BP (IGAN_{AMS} 7821) significantly differs from the previously reported date 41540–39470 cal BP (Beta 159972) from the same location in Section 5. In both samples, dated material is contaminated with foreign carbon, which cannot be separated by applying modern pre-treatment techniques. These are apparent dates that reflect neither the age of the parent material nor the time of their redeposition and further pedogenesis. Today, the reported OSL date 37.0 ± 3.1 ka (GdTL 3424) is an available chronological benchmark that predates formation of the last ice-dammed lake in the Chuya basin and its cataclysmic draining.

4.2 Establishing the chronology and paleoenvironmental conditions of soil formation within the highlands of the SE Altai.

Today, the oldest reasonably described paleosols within the SE Altai are dated by applying radiocarbon method to the early Holocene – 10–11 ka cal BP (Agatova *et al.*, 2016; Bronnikova *et al.*, 2018). In this context reported by Herget (2005, p. 36), uncalibrated ^{14}C age 35870 ± 490 BP (Beta 159972) of “a layer of organic sediment, probably a part of paleosol profile” in Section 5 is very important information. Our results of micro- and macro-morphological analysis of sediments in this location indicate that studied substrate was affected by pedogenesis: The former day surface of the sliding loam pack, before it was washed out by the waters of the ice-dammed lake and covered by diluvium, experienced cryogenesis and solifluction under cold and humid conditions. It could be stated that under cross-bedded deposits of cataclysmic flood, only the middle horizon of paleosol profile has been preserved without the eroded top humus accumulating layer.

The Paleogene–Neogene age of organic matter, which was redeposited and served as parent substrate for the Pleistocene pedogenesis, is confirmed by various proxy data presented above. Dated substrate is related to a mix-

ture of heterogeneous and heterochronous organic matter pools. Even though the radiocarbon date 41540–39470 cal BP (Beta 159972) falls within the Pleistocene epoch, this is an apparent age. Detected pollen and nonpollen palynomorphs of Quaternary appearance, including *Lemna*, *Potamogeton*, sponges, *Botriococcus*, indicate the aquatic environment at some stages of sedimentation and argue for “young” carbon influx into the redeposited Paleogene–Neogene material. Absence of the upper part (humus-accumulating horizon) of soil profile in Section 5 could be explained by the winnowing activity of ice-dammed lakes and/or its erosion by cataclysmic outburst floods. Cryoturbation is another process that affected the destruction of studied soil-sedimentary sequence. It occurred both during and after soil formation.

Generally, for the first time, our multidisciplinary investigations reasonably demonstrate the possibility of pedogenesis within the high mountain basins of the Russian Altai between periods of ice-dammed lake accumulation. Soil formation is one of the processes leading to the contamination of the ancient (Jurassic, Cretaceous, Paleogene, and Neogene) organic matter with “young” carbon – not only at the present time and in the Holocene, but also in the Pleistocene.

Examples of the redeposition of ancient organic matter into the Pleistocene sediments are presented in sections 4 and 3 in the Kurai basin (Figs. 6 and 7). The first one is a layer of organic material (described as fossil soil (Rogozhin *et al.*, 2008)) buried by alluvium within the terrace of the right tributary of the Chuya River. Radiocarbon date 23420–22110 cal BP IGAN 3204 for this layer is one of a few that falls within the last (Sartan or MIS-2) glaciation in the SE Altai, but formation of such humus-rich soil is in poor agreement with the paleoenvironment of that time. Cleaning of the larger area of the outcrop and re-examination of Section 4 revealed inter-bedding of alluvial and peat layers. Further radiocarbon dating demonstrated inversion of obtained ages. Sedimentation patterns in this location argue for periodical river bed migration and accumulation of eroded peat-rich sediments during the post-glacial period. Like in previous examples, washed-out Paleogene–Neogene coal-bearing deposits most likely served as a source of organic matter. Similarly, in Section 3, a layer of peaty material was ^{14}C dated 40930–35820 cal BP (SOAN 9505). Nevertheless, the OSL ages (11.12 ± 1.74 ka, GdTL-3126 and 9.41 ± 1.68 ka, GdTL-3125) of sands bracketing this peaty layer indicate the early Holocene age of lacustrine sedimentation.

Apparent (aged) radiocarbon date (17710–16210 cal BP, IGAN 6249) for buried soils was obtained in Section 6 located in the small erosion valley, which cuts the Bigdon Hills (Fig. 10). The opportunity to verify this date arose due to finding of lenses with charcoals lying stratigraphi-

cally lower in the same section. Radiocarbon dating of charcoals and enclosing substrate shows the early Holocene ages (10–11 ka cal BP). Charcoals indicate the presence of the tree vegetation with diffuse-porous wood, most likely being birch or poplar. Radiocarbon age of charcoals is younger than the age of the enclosing substrate. It suggests a similar mechanism for the influx of ancient organic material in the upper alluvial–colluvial pack as a result of the redeposition of the Paleogene–Neogene substrate covering the Bigdon Hills.

The analysis of available radiocarbon dates for Pleistocene buried soils in the region indicates the contamination of the samples by foreign carbon. It does not allow to determine the time of the late Pleistocene pedogenesis. Presented OSL age 37.0 ± 3.1 ka (GdTL 3424) is a reliable date that predates the oldest known Pleistocene pedogenesis in the Chuya basin.

4.3 Estimating the range and magnitude of the tectonically driven topography rebuilding in the post-Neogene time.

For clarifying the Cenozoic and particularly the Quaternary tectonic history of the SE Altai, understanding the extent and distribution patterns of the Paleogene–Neogene boggy–lacustrine sedimentation in the region is of vital importance (Devyatkin, 1965; Luzgin and Rusanov, 1992; Agatova *et al.*, 2017; Rusanov *et al.*, 2017). Acceptance of apparent ^{14}C dates of lithified peat–brown coal layers with unbroken structure in sections 8a, b (Figs. 11 and 12) in the Dzhazator valley as being valid ones could have resulted in incorrect interpretation of previously unknown near-surface location of the Paleogene–Neogene deposits (Agatova *et al.*, 2017). They could be mistaken for the Pleistocene deposits with the redeposited ancient pollen. As a result, information on the locations of the Paleogene–Neogene sediments will be missed. Today, such information allows understanding both Paleogene–Neogene tectonic plan and the post-Neogene tectonically driven topography rebuilding in this highest part of the Altai Cenozoic uplift.

Originally, based on the geomorphic position of Section 8c in the Dzhazator valley, the Holocene age of the peat–mineral layers was assumed. However, the first numerical dating results for thick peaty-rich layers showed the MIS-2 age of studied deposits. In regional paleogeography, it corresponds to the last glaciation. Thus, such discrepancy has cast doubt on the validity of the obtained dates. Further numerous radiocarbon dating revealed large scattering of ^{14}C ages and their inversion, which encouraged multidisciplinary investigations of dated substrate, as well as areal geomorphological investigations to detect the possible source of ancient organic matter (Agatova *et al.*, 2017, 2019). It results in the discovery of previously unknown location of the Upper Oligocene–Lower Miocene brown coal deposits in the Russian Altai (Agatova *et al.*, 2017).

We also demonstrate that radiocarbon ages contradict to paleontological and geochemical characteristics of sediments (Agatova *et al.*, 2019).

In general, different degrees of transformation of the organic material (from the least changed, horizontally bedded, to creased into folds or crashed with broken inner structure and high content of mineral matter) are exhibited in the upper, middle, and lower parts of the sliding slope (sections 8a, 8b, and 8c, respectively). The paleontological and geochemical characteristics clearly indicate the formation of organic material in the Paleogene–Neogene time under the humid meadow–boggy conditions and warm climate. Significant scattering of obtained radiocarbon dates for studied sediments was revealed – ^{14}C ages measured in three different laboratories ranged between 16.0 and 50 ka cal BP (Fig. 2, Table 1). Such valuable scattering, inversion of radiocarbon ages within a section, and discrepancy with other proxy data indicate mixing of heterochronous carbon in OM in individual for each sample proportion. It is a common result of active tectonics and complicated sedimentary history. Like in the above cases, obtained radiocarbon dates are apparent ages, which could not be used as chronological markers. Nevertheless, dating results encourage further detailed study of dated material, as well as areal geological geomorphological investigations.

5. Conclusion

Multidisciplinary investigations within the SE Altai set a problem of obtaining apparent radiocarbon ages for organic matter, which represent a mix of geological (with the age of several million years) and young carbon. Such mixture in unique for each sample proportions could not be separated today by utilizing standard pre-treatment techniques. The organic-rich Middle and Upper Carboniferous, Lower Jurassic, Paleogene, and Neogene deposits are the sources

of old carbon of geological age in the region. Active tectonic movements caused re-exposure of these deposits and their further redeposition as a result of numerous exogenous processes.

Within the SE Altai, the Paleogene–Neogene organic-rich lacustrine and boggy–lacustrine deposits are mainly distributed at the foot of the Kurai range in the western and northwestern parts of the Chuya basin. They are exposed at the surface and, according to drilling and geophysical data, are traced under Quaternary sediments. There are also exposures of ancient organic-rich deposits along the south side of the South-Chuya range and to a less degree in some other places in the region. Correct interpretation of ^{14}C dates for paleosols and organic-rich sediments in these locations demands understanding of the origin and sources of dated organic matter. All radiocarbon dates presented in this article are related to a mixture of heterogeneous and heterochronous organic matter pools and cannot be applied for chronological reconstructions of the Late Quaternary climatic and nature events.

Obtaining of apparent radiocarbon ages as a result of contamination of dated substances with extraneous carbon is a quite common problem for tectonically active mountain provinces, although methodological studies in the Russian Altai have not yet been carried out earlier. Within the SE Altai, ancient sediments, affected by short-distant transportation and redeposition, preserve their main paleontological and mineralogical features. It gives an opportunity to verify obtained radiocarbon dates by various proxy data. Without such verification, single ^{14}C dates could hardly serve as reliable chronological markers.

Acknowledgement

The study was supported by State assignment of IGM SB RAS and partly funded by RFBR foundation (Grant No. 18-05-00998).

References

- Agatova AR, Nepop RK, Bronnikova MA, Slyusarenko IYu and Orlova LA, 2016. Human occupation of South Eastern Altai highlands (Russia) in the context of environmental changes. *Archaeological and Anthropological Sciences* 8: 419-440, DOI: [10.1007/s12520-014-0202-7](https://doi.org/10.1007/s12520-014-0202-7).
- Agatova AR, Nepop RK, Rudaya NA, Khazina IV, Zhdanova AN, Bronnikova MA, Uspenskaya ON, Zazovskaya EP, Ovchinnikov IY, Panov VS and Shurygin BN, 2017. Discovery of Upper Oligocene–Lower Miocene brown coal deposits (Kosh-Agach formation) in the Dzhazator River valley (Southeastern Russian Altai): Neotectonic and paleogeographical aspects. *Doklady Earth Sciences* 475(2): 854-857, DOI: [10.1134/S1028334X17080104](https://doi.org/10.1134/S1028334X17080104).
- Agatova AR and Nepop RK, 2017. Pleistocene glaciations of the SE Altai, Russia, based on geomorphological data and absolute dating of glacial deposits in hagan reference section. *Geochronometria* 44: 49-65, DOI: [10.1515/geochr-2015-0059](https://doi.org/10.1515/geochr-2015-0059).
- Agatova AR, Nepop RK, Zazovskaya EP, Ovchinnikov IYu and Moska P, 2019. Problems of developing the Pleistocene radiocarbon chronology within high mountain terrains by the example of Russian Altai. *Radiocarbon* 61(6): 2019-2028, DOI: [10.1017/RDC.2019.83](https://doi.org/10.1017/RDC.2019.83).

- Agatova AR, Nepop RK, Carling PA, Bohorquez P, Khazin LB, Zhdanova AN and Moska P, 2020. Last ice-dammed lake in the Kuray basin, Russian Altai: New results from multidisciplinary research. *Earth-Science Reviews*, DOI: [10.1016/j.earscirev.2020.103183](https://doi.org/10.1016/j.earscirev.2020.103183).
- Arslanov AA, 1987. *Radiocarbon: Geochemistry and Geochronology*. Leningrad: Leningrad State University Press (in Russian).
- Beug HJ, 2004. *Leitfaden der Pollenbestimmung für Mitteleuropa und angrenzende Gebiete*. München.
- Bronk Ramsey C, 2017. Methods for Summarizing Radiocarbon Datasets. *Radiocarbon* 59(2): 1809-1833, DOI: [10.1017/RDC.2017.108](https://doi.org/10.1017/RDC.2017.108).
- Bronnikova MA, Agatova AR, Lebedeva MP, Nepop RK, Konopljanikova YuV and Turova IV, 2018. Record of Holocene Changes in High-Mountain Landscapes of Southeastern Altai in the Soil-Sediment Sequence of the Boguty River Valley. *Eurasian Soil Science* 51(12): 1381-1396, DOI: [10.1134/S1064229318120037](https://doi.org/10.1134/S1064229318120037).
- Buslov MM, Zykin VS, Novikov IS and Delvo D, 1999. Structural and geodynamic features of Cenozoic formation of Chuya intermountain depressions, Gorny Altai. *Russian Geology and Geophysics* 40(12): 1720-1736, DOI: [10.1016/j.rgg.2011.12.007](https://doi.org/10.1016/j.rgg.2011.12.007).
- Butvilovsky VV, 1993. *Paleogeography of the Last Glaciation and the Holocene of Altai: A Catastrophic Events Model*. Tomsk, Tomsk University Press (in Russian).
- Deev, EV, Nevedrova, NN, Zol'nikov, ID, Rusanov, GG, and Ponomarev, PV, 2012. Geoelectrical studies of the Chuya basin sedimentary fill (Gorny Altai). *Russian Geology and Geophysics* 53(1): 92-107, DOI: [10.1016/j.rgg.2011.12.007](https://doi.org/10.1016/j.rgg.2011.12.007).
- Devyatkin, EV, 1965. *Cenozoic deposits and neotectonics of South-eastern Altai*. Moscow, USSR Academy of Science (In Russian).
- Dobretsov, NL, Buslov, MM, Delvaux, D, Berzin, NA, and Ermikov, VD, 1996. Meso- and Cenozoic tectonics of the Central Asian mountain belt: effects of lithospheric plate interaction and mantle plumes. *International Geology Review* 38(5): 430-466, DOI: [10.1080/00206819709465345](https://doi.org/10.1080/00206819709465345).
- Galbraith, RF, Roberts, RG, Laslett, GM, Yoshida, H, and Olley, JM, 1999. Optical dating of single and multiple grains of quartz from Jinminum Rock Shelter, Northern 12 Australia. Part I, experimental design and statistical models. *Archaeometry* 41: 1835-1857.
- Glorie, S, De Grave, J, Buslov, MM, Zhimulev, FI, Izmer, A, Vandoorne, W, Ryabinin, A, Van den haute, P, Vanhaecke, F, and Elburg, MA, 2011. Formation and Palaeozoic evolution of the Gorny-Altai–Altai-Mongolia suture zone (South Siberia): Zircon U/Pb constraints on the igneous record. *Gondwana Research* 20(2-3): 465-484, DOI: [10.1016/j.gr.2011.03.003](https://doi.org/10.1016/j.gr.2011.03.003).
- Glorie, S, De Grave, J, Buslov, MM, Zhimulev, FI, and Elburg, MA, 2012. Structural control on Meso-Cenozoic tectonic reactivation and denudation in the Siberian Altai: Insights from multi-method thermochronometry. *Tectonophysics* 544: 75-92, DOI: [10.1016/j.tecto.2012.03.035](https://doi.org/10.1016/j.tecto.2012.03.035).
- Gribenski, N, Jansson, KN, Lukas, S, Stroeve, AP, Harbor, JM, Blomdin, R, Ivanov, MN, Heyman, J, Petrakov, DA, Rudoy, A, Clifton, T, Lifton, NA, and Caffee, MW, 2016. Complex patterns of glacier advances during the late glacial in the Chagan Uzun Valley, Russian Altai. *Quaternary Science Reviews* 149: 288-305, DOI: [10.1016/j.quascirev.2016.07.032](https://doi.org/10.1016/j.quascirev.2016.07.032).
- Guerin, G., Mercier, N, and Adamiec, G, 2011. Dose-rate conversion factors: update. *Ancient TL* 29: 5-8.
- Herget, J, 2005. Reconstruction of Pleistocene Ice-dammed Lake Outburst Floods in Altai-mountains, Siberia. *Geological Society of America*, Special Publication 386: 118pp.
- Herget, J, Agatova, AR, Carling, P, and Nepop, RK, 2020. Altai megafloods - the temporal context. *Earth Science Reviews* 200, 102995, DOI: [10.1016/j.earscirev.2019.102995](https://doi.org/10.1016/j.earscirev.2019.102995).
- Jankovska, V, and Komarek, J, 2000. Indicative value of *Pediastrum* and other Coccal Green algae in palaeoecology. *Folia Geobotanica* 35: 59-82, DOI: [10.1007/BF02803087](https://doi.org/10.1007/BF02803087).
- Kuprianova, LA, and Alyoshina, LA, 1972. *Spore and pollen of plants in European part of the USSR*. Leningrad, Nauka (in Russian).
- Luzgin, B.N, and Rusanov, GG, 1992. Characteristics of formation of Neogenic deposits in the Southeastern Gorny Altai. *Russian Geology and Geophysics* 33(4): 18-23.
- Murray, AS, and Wintle, AG, 2000. Luminescence dating of quartz using an improved single-aliquot regenerative-dose protocol. *Radiation measurements* 32(1): 57-73, DOI: [10.1016/S1350-4487\(99\)00253-X](https://doi.org/10.1016/S1350-4487(99)00253-X).
- Narozhny, YuK, Osipov, AV, 1999. Oroclimatic conditions of the Central Altai glaciations. *News of Russian Geographical Society* 131(3): 49-57 (in Russian).
- Nekhoroshev, VP, 1966. *Tectonics of Altai*. Moscow: Nedra (in Russian).
- Nevedrova, NN, Epov, MI, Antonov, EY, Dashevsky, YA, and Duchkov, AD, 2001. Deep structure of the Chuya basin (Gorny Altai), as imaged by TEM soundings. *Russian Geology and Geophysics* 42(9): 1399-1416.
- Novikov, IS, 2004. *Morfotektonika Altaja* (Morphotectonics of the Altai Mountains). Novosibirsk, SO RAN Publisher, "Geo" Brunch: 313pp (in Russian).
- Okishev, PA, and Borodavko, PS, 2001. New materials on the history of the Chuya-Kurai limnosystem. *Issues of Geography of Siberia* 24: 18-27 (in Russian).
- Ostanin, OV, 2007. Modern evolution of high mountain systems (by the example of Central and Southeastern Altai). PhD thesis. Barnaul Altai State University, 195pp (in Russian).
- Permafrost-hydrogeological Map, scale 1:200000, 1977. Novosibirsk, Department of Funds Western *Siberian Geological administration*, 18195.
- Prescott, JR, and Stephan, LG, 1982. *The contribution of cosmic radiation to the environmental dose for thermoluminescence dating. Latitude, altitude and depth dependencies*. *TLS II-1*: 16-25.
- Reimer, PJ, Bard, E, Bayliss, A, Beck, JW, Blackwell, PG, Bronk Ramsey, C, Buck, CE, Cheng, H, Edwards, RL, Friedrich, M, Grootes, PM,

- Guilderson, TP, Hafliadason, H, Hajdas, I, Hatté, C, Heaton, TJ, Hogg, AG, Hughen, KA, Kaiser, KF, Kromer, B, Manning, SW, Niu, M, Reimer, RW, Richards, DA, Scott, EM, Southon, J.R., Turney, CSM, and Van der Plicht, J, 2013. IntCal13 and MARINE13 radiocarbon age calibration curves 0-50000 years cal BP. *Radiocarbon* 55(4): 1869-1887, DOI: [10.2458/azu_js_rc.55.16947](https://doi.org/10.2458/azu_js_rc.55.16947).
- Rogozhin, EA, Ovsyuchenko, AN, and Marahanov, AV, 2008. Major earthquakes of the southern Gorny Altai in the Holocene. *Izvestiya. Physics Solid Earth* 44(6): 469-486, DOI: [10.1134/S1069351308060037](https://doi.org/10.1134/S1069351308060037).
- Rudoy, AN, 2002. Glacier-Dammed Lakes and geological work of glacial superfloods in the Late Pleistocene, Southern Siberia, Altai Mountains. *Quaternary International* 87(1): 119-140, DOI: [10.1016/S1040-6182\(01\)00066-0](https://doi.org/10.1016/S1040-6182(01)00066-0).
- Rudoy, AN, 2005. *Giant Current Ripples*. Tomsk, Tomsk State University (in Russian).
- Rusanov, GG, Deev, EV, Zolnikov, ID, Khazin, LB, Khazina, IV, and Kuz'mina, O.B, 2017. Reference section of Neogene-Quaternary deposits in the Uimon Basin (Gorny Altai). *Russian Geology and Geophysics* 58(8): 973-983, DOI: [10.1016/j.rgg.2017.07.008](https://doi.org/10.1016/j.rgg.2017.07.008).
- Selin, PF, Goverdovsky, VA, 2000. *Coal deposits of the Altai Republic. The results and prospects of the geological study of the Altai Mountains*. Gorno-Altai, Gorno-Altai Publishing House (in Russian).
- Shokalsky, SP, Zybin, VA, and Sergeev, VP, 1999. *Legend of the Altai series of the State Geological Map of the Russian Federation - 1: 200000. Explanatory note*. Novokuznetsk, OF FUGUP (in Russian).
- Shumilovskikh LS, Schlüt F, Achterberg I, Bauerochse A, and Leuschner HH, 2015. Nonpollen palynomorphs from mid-Holocene peat of the raised bog Borsteler Moor (Lower Saxony, Germany). *Studia Quaternaria* 32(1): 5-18, DOI: [10.1515/squa-2015-0001](https://doi.org/10.1515/squa-2015-0001).
- Skripkin, V, and Kovaliukh, N, 1997. Recent Developments in the Procedures Used at the SSCER Laboratory for the Routine Preparation of Lithium Carbide. *Radiocarbon* 40(1): 211-214, DOI: [10.1017/S0033822200018063](https://doi.org/10.1017/S0033822200018063).
- Skrypnikova, M, Uspenskaya, O, and Khokhlova, O, 2011. Paleoclimate Study of Mountain Ecosystems by Multiple Group Biological Analysis. *Journal of Mountain Science* 8: 24-36, DOI: [10.1007/s11629-011-1033-y](https://doi.org/10.1007/s11629-011-1033-y).
- Solotchina, EP, 2009. *Structural Typomorphism of Clay Minerals of Sedimentary Sections and Crusts of Weathering*. Novosibirsk, Geo (in Russian).
- Svitoch, AA, Boyarskaya, TD, Voskresenskaya, TN, Glushakova, II, Evseev, AV, Kursalova, VI, Parmonova, NN, Faustov, SS, and Khorev, VS, 1978. *The sections of the latest deposits of Altai*. Moscow, MSU Publisher (in Russian).
- Uspenskaya, ON, 1986. Other algae In: Treshnikov AF, Kvasov VA, Rumjancev VA ed. *General patterns of formation and development of lakes. Methods of studying the history of lakes*. Leningrad, Nauka: 146-151 (in Russian).
- Wallinga, J. 2002. On the detection of OSL age overestimation using single-aliquot techniques. *Geochronometria* V21: 17-26.
- Vysotsky, EM, 2009. The age of relief forming of weelhead part of Kurai depression (Gorny Altai). In: *Proceedings of the VI All-Russian Quaternary conference "Fundamental Problems of Quaternary: Results and Trends of Future Researches"*, Novosibirsk, SB RAS Publisher: 137-138 (in Russian).
- Zolnikov, ID, 2011. *Role of glaciations and glacial megafloods in geological structure of the Neopleistocene sedimentary complexes in Gorny Altai and Altai foreplain*. Doctoral Thesis. Novosibirsk: OIT IPGG SB RAS, 35p. (in Russian).
- Zolnikov, ID, Mistrukov, AA, 2008. *Quaternary deposits and relief of the Chuya and Katun valleys*. Novosibirsk, Parallel (in Russian).
- Zolnikov, ID, Deev, EV, Kotler, SA, Rusanov, GG, Nazarov, DV, 2016. New results of OSL dating of Quaternary sediments in the Upper Katun'valley (Gorny Altai) and adjacent area. *Russian Geology and Geophysics* 57(6): 933-943, DOI: [10.1016/j.rgg.2015.09.022](https://doi.org/10.1016/j.rgg.2015.09.022).